Bull. Mater. Sci., Vol. 38, No. 1, February 2015, pp. 1–12. © Indian Academy of Sciences.

Influence of thermo-mechanical processing on microstructure, mechanical properties and corrosion behavior of a new metastable β-titanium biomedical alloy

MOHSIN TALIB MOHAMMED[1,*], ZAHID A KHAN[1], M GEETHA[2], ARSHAD N SIDDIQUEE[1] and PRABHASH MISHRA[3]

[1]Mechanical Engineering Department, Jamia Millia Islamia, New Delhi 110 025, India
[2]Centre for Biomaterials Science and Technology, VIT University, Vellore 632 014, India
[3]Nano-Sensor Research Laboratory, Faculty of Engineering and Technology, Jamia Millia Islamia, New Delhi 110 025, India

MS received 18 April 2014; revised 30 June 2014

Abstract. **This paper presents the results on the influence of different thermo-mechanical processing (TMP) on the mechanical properties and electrochemical behavior of new metastable β-alloy Ti–20.6Nb–13.6Zr–0.5V (TNZV). TMP included hot working in below β-transus, solution heat treatments at same temperature in different cooling rates in addition to aging. Depending upon the TMP conditions, a wide range of microstructures with varying spatial distributions and morphologies of equiaxed/elongated α, β phases were attained, allowing for a wide range of mechanical and electrochemical properties to be achieved. The corrosion behavior of studied alloy was evaluated in Ringer's solution at 37°C using open-circuit potential-time and potentiodynamic polarization measurements.**

Keywords. **Titanium alloys; biomedical applications; microstructure; mechanical properties; corrosion.**

1. Introduction

In the field of biomaterials, metallic implant materials such as stainless steels, cobalt–chromium-based alloys and titanium (Ti) materials have made a significant impact in the last decades especially in applications requiring mechanical and electrochemical properties. Among metallic materials, Ti and its alloys are extensively used in a variety of applications like aerospace, chemical industries, power plants, medical prostheses[1] owing to their good mechanical properties and corrosion resistance.[2] They are considered the best choice for replacing or repairing failed hard tissues (structural biomedical applications) as these materials present excellent biocompatibility, high strength to density ratio, outstanding corrosion resistance due to an oxide layer formation on surface as well as low modulus of elasticity that is closer to bones than biomedical stainless steels and cobalt–chromium alloys, decreasing risk of catastrophic failure during prostheses service life.[1–7]

Commercial pure Ti (CP) (ASTM F-67, ISO 5832-2) and Ti–6Al–4V (ASTM F-1472, ASTM F-136, ISO 5832-3)[8,9] are the most well known Ti materials used in biomedical applications. CP-Ti is used extensively in dental applications and found not suitable for load-bearing applications owing to its poor mechanical properties such as low shear strength. The α + β type Ti–6Al–4V alloy has been used as structural biomaterial for manufacturing orthopedic prostheses as well as dental implants because of its excellent specific strength, corrosion resistance and biocompatibility characteristics.[5,6] However, the alloying elements present in this alloy have their own adverse effect in biomedical environment. The literature also proves that the presence of vanadium (V) ions in human tissues can alter the kinetics of the enzyme activity associated with the inflammatory response cells.[10,11] The presence of aluminum (Al), on the other hand, increases the potential for the development of Alzheimer's disease[11–13] especially during long-term implantation. Additionally, one of the most important properties which pose serious limitations on the performance of Ti alloys as implant materials for artificial joints (e.g. hip, knee, shoulder joints, etc.) is its higher modulus of elasticity. It is essential that the stiffness of the implant material be as close as possible to the connected bone. This characteristic facilitates an effective transfer of mechanical stress, by providing stress shielding effect, through the interface from the implant to the adjacent bone and avoids the damage of bone cells.[14] When there is a large difference between the stiffness of the two, it may cause osteoporosis or poor osseointegration (poor bone–Ti implant contact integration)[15] which may consequently lead to crack nucleation and an eventual failure of the implant.[16] Ti–6Al–4V alloy has a modulus of

*Author for correspondence (mohsent123@yahoo.com)

approximately 110 GPa,[17] which is extensively higher than that of human bone (10–40 GPa).[2,18,19] The high modulus of Ti–6Al–4V is as a result of high amount of Al content which leads to increase in the volume fraction of α-phase.[2]

Multifunctional β-type Ti alloys which are widely used in various biomedical applications have been developed all over the world. In recent times, some new near β-type Ti alloys containing β-stabilizers such as Nb and Zr have attracted much special attention for orthopedic implants applications owing to their unique combination of better mechanical properties, low elastic modulus, superior biocorrosion resistance, nontoxicity against osteoblastic cells, non-allergic problems and excellent biocompatibility. The required mechanical properties in this kind of Ti alloys can be improved due to solid solution and second phase strengthening while preserving the light weight characteristics of Ti.[20,21] From crystallographic insight, the body centered cubic structure (bcc) of β-phase shows higher symmetry as compared with the hexagonal closed packing (hcp) α-phase resulting in an isotropic mechanical behavior. Moreover, it is found that their elastic modulus can be significantly reduced by adjusting the concentration of β-stabilizing elements[22–24] which makes them appropriate for load-bearing surgical implants. On other hand, this type of Ti alloys exhibits extraordinary corrosion resistance in human body fluid. This behavior is due to the formation of a protective, hard and tightly adherent oxide film.[25] This oxide film offers chemical inertness to the Ti implants in human body fluid and guarantees its biocompatibility as a biomaterial. Therefore, Ti-based alloys with nontoxic and non-allergic elements such as Nb, Zr and other elements have been widely used to design new β-type Ti alloys.[26] It is well known that Nb is β-stabilizer element and it forms homogeneous solid solution with Ti in all kinds of Ti alloys when alloyed within certain concentration,[27–29] while Zr is traditionally judged as a neutral element in the α- and α + β-type alloys. On the other hand, it is pointed out that Zr can be treated as a kind of β-stabilizer in the Ti–Nb–Zr alloy system as this element could inhibit α precipitation according to Tang *et al*[30] and Ribeiro *et al*[31] and also reduce the martensitic transformation start temperature (M_s) considerably.[32,33] In this regard, the addition of Nb and Zr is preferable to develop absolutely safe Ti-based alloys for biomedical applications depending upon its ability to achieve biological passivity and capacity of reducing the elastic modulus.[34]

In general, thermo-mechanical processing (TMP) is a metallurgical process that integrates work hardening and heat treatment into a single process[35] plays a crucial role to produce a microstructure with outstanding properties in the materials.[36–38] The mechanical properties[39] as well as corrosion behavior[40] depend strongly on the alloy composition, processing history, heat treatment conditions which decide the varieties of microstructures. Near-β Ti alloys respond to thermal treatment and TMP and various microstructural constituents like the size, shape and the amount of the various phases can be modified by varying the TMP parameters. However, the influence of thermal treatment and TMP on microstructural features of as-cast Ti–Nb–Zr alloy system and in turn on its mechanical and electrochemical behavior is scarcely reported. Indian researchers[40] studied the effect of heat treatment on the corrosion behavior of Ti–13Zr–13Nb alloy (ASTM F 1713-96) in Ringer's solution. They found that water quenched α + β alloys possess superior corrosion resistance due to a homogeneous distribution of alloying elements. The role of TMP on microstructure, mechanical properties and corrosion behavior in simulated body fluid of Ti–13Nb–13Zr alloy (TNZ) has been investigated by Majumdar *et al*.[41,42] It is found that the major results were mainly depending upon the cooling rate after solution treatment. The presence of high amount of α phase in the microstructure showed high elastic modulus and lower corrosion potential (E_{corr}) whereas the presence of α'' martensite and retained β-phases lowered the modulus of the samples and caused further decrease in corrosion potential.

Nowadays, great efforts in terms of extensive work and focus is being dedicated by engineers and materials scientists in developing novel Ti alloys for biomedical applications with low elastic modulus and superior electrochemical behavior. In this study, titanium–niobium–zirconium-based alloy containing small amounts of vanadium was investigated in order to evaluate its possible application as a biomedical material. Niobium, zirconium and vanadium, having a β-phase stabilizing effect for titanium materials, were chosen to control microstructure desirably. Microstructure control was carried out by performing hot working in α + β field and subsequently heat treatment at same temperature in different cooling rates. Finally, the relationship between thermomechanical processing, mechanical properties and corrosion behavior were revealed and are discussed in detail.

2. Material and methods

The alloy in the present investigation was cast using the mixture of sponge Ti along with niobium powder and zirconium chips as raw materials. The Ti–20.6Nb–13.6Zr–0.5V (TNZV) alloy was prepared using the non-consumable vacuum arc melting technique and supplied in the form of 600 g pancakes. The pancakes were re-melted three times to ensure compositional homogeneity. The composition of the alloy was analyzed and the same in wt% is given in table 1.

The as-cast TNZV alloy was then heat treated at 1000°C for 1 h for homogenization, water cooled. Subsequently, the homogenized samples were given 10% reduction by forging at below the β-transition temperature (650°C) and directly subjected to 25% reduction by rolling at same temperature and were then air cooled to room temperature. After entire

Table 1. The chemical composition (wt%) of TNZV alloy used in this study.

Ti (wt%)	Nb (wt%)	Zr (wt%)	V (wt%)	Fe (wt%)
Balance	20.6	13.6	0.5	0.14

plastic deformation the alloy remained free from any of the metal working defects which indicated that the entire metal working process was performed successfully.

The hot deformed TNZV samples were solution treated at 650°C (below β-transus) for 1 h in a dynamic argon atmosphere; this was followed by water quenching (WQ), air cooling (AC) or furnace cooling (FC). Aging treatment was done only on the water quenched samples at 500°C for 5 h. The TMP route of TNZV alloy is shown schematically in figure 1.

The composition of the major and trace elements was determined using X-ray fluorescent (XRF) spectrometer (Oxford-X Srata, model: ISIS 1559). Microstructure analysis of the heat treated samples was carried out using an optical microscope and field emission scanning electron microscope (FE-SEM,NOVA NANO SEM 450 FEI, The Netherlands) at 2 kV. For this, the metallographic samples were prepared using standard techniques for Ti and its alloys.[43] They were ground to 1200 grit with silicon carbide (SiC), followed by final polishing to a mirror finish using 0.5 μm diamond paste. The metallographically polished samples were etched with Kroll's reagent (10 vol% HF and 5 vol% HNO_3 in water). Room temperature X-ray diffraction analysis was carried out on an X-ray Diffractometer, Philips, Holland, PW 1830 with Cu Kα radiation (wavelength 1.54056 Å) at an accelerating voltage of 40 kV and a current of 30 mA.

Vickers microhardness measurements were performed using a computer-controlled precision microhardness tester (*model*: *MicroWhizHard*; make: Mitutoyo, Japan) with an indentation load of 300 gf and a dwell time of 5 s for each of the indents. Ten indentations were taken for each specimen and the average values were considered. Hardness measurements were carried out on the samples finished using 0.5 μm diamond paste.

Tensile testing was performed as per ASTM E8M to determine the ultimate tensile strength (UTS), 0.2% off-set yield strength (YS) and elongation (*e*%) using a conventional tensile testing unit (computerized FIE Make Universal Testing Machine, *Model: UTE-60*), with a constant cross-head speed of 1 mm min^{-1} in air at room temperature. Dog-bone-shaped tensile specimens with dimensions as shown in figure 2 were precisely machined using wire electrical discharge machine (*Wire-EDM*). After machining, tensile specimens were polished using SiC waterproof papers of up to #2500 grit and the gage length of the specimens was mechanically polished using a diamond paste with a particle size 0.5 μm.

The corrosion behavior of the TNZV alloy was studied using potentiostat comprising of three-electrode cell with an Ag/AgCl (KCl saturated) as the reference electrode (all the potential measurements were made with reference to it) and a platinum foil as the counter electrode (cathode). The test specimens with dimensions (10 ×10 ×2 mm) were served as a working electrode (anode). Anodic polarization was carried out with a corrosion measuring system (model: WPG100e, Korea) which was computer interfaced through relevant software named *Sequencer* version 5. The OCP and passive current density were used as the criterion for evaluating the corrosion characteristics of the thermo-mechanically processed Ti alloy.

The surface area exposed to the electrolyte was 0.126 cm^2. For each experiment, the specimens were prepared by sequential grinding with water-proof emery paper up to 2000 grit SiC, followed by polishing with alumina of 0.5 μm for getting high mirror surface finish and then cleaning in an

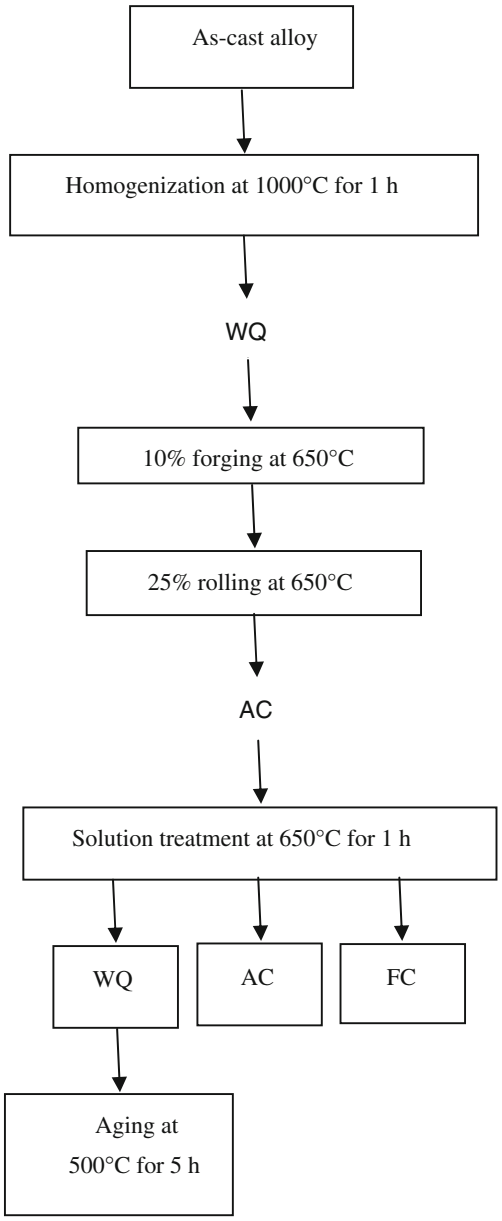

Figure 1. Schematic diagram of the thermo-mechanical processing of TNZV alloy.

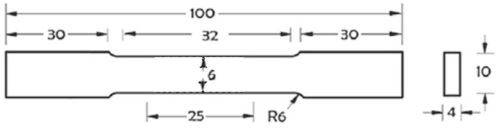

Figure 2. Dimensions of tensile specimen proportional to the ASTM E-8 standard.

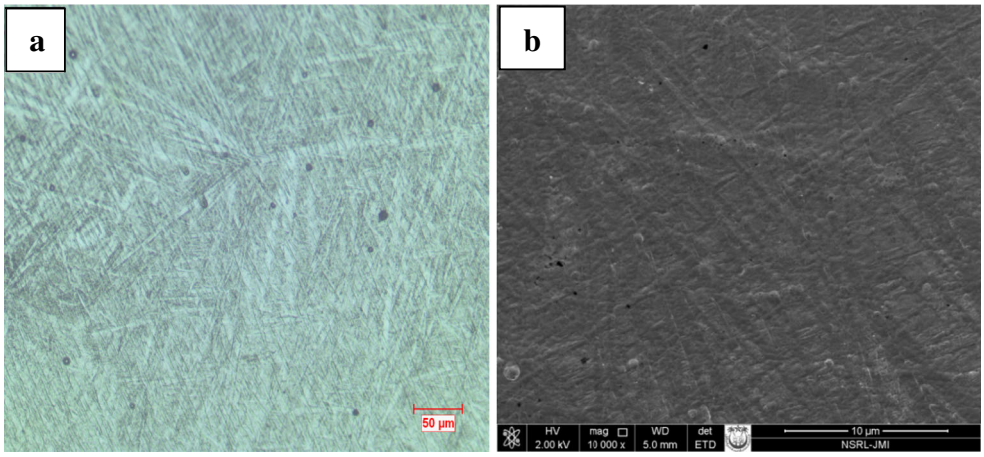

Figure 3. Microstructure of as-cast TNZV alloy: (**a**) optical micrograph and (**b**) scanning electron microstructure (SEM).

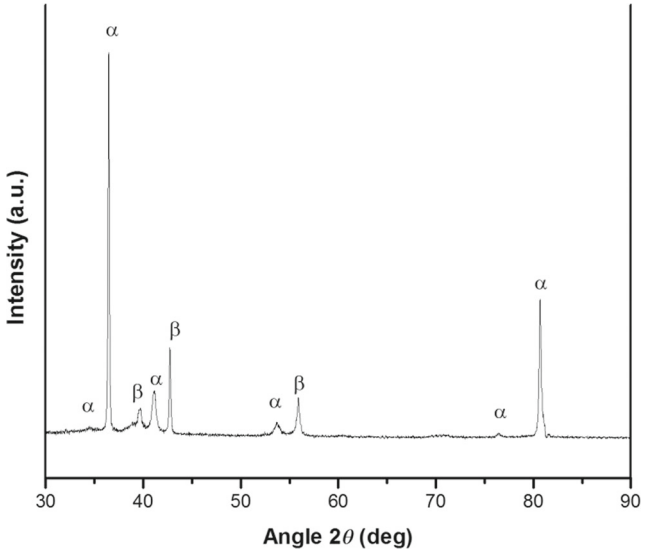

Figure 4. X-ray diffraction profiles of as-cast TNZV alloy.

ultrasonic bath for three times. Freshly prepared Ringer's solution was used as the electrolyte for each experiment to simulate physiological conditions representative of what a biomedical component would experience.[1,44–46] The solution had the following chemical composition dissolved in one liter of distilled water: 9.00 g NaCl, 0.43 g KCl, 0.20 g $NaHCO_3$ and 0.24 g $CaCl_2$. The pH of the solution was maintained at 7.4. The solution was naturally aerated and kept at 37 ± 1°C throughout the tests. Upon immersion of the specimens into the electrolyte, the OCP was measured as a function of time, until the stable value was reached. Consequently, corrosion potential (E_{corr}) and passive current density (I_{corr}) of the alloy were determined from the potential *vs.* current density polarization curve. The polarization curves were obtained with a scan rate of 0.166 mV s^{-1} in the range from −750 to 2500 mV (Ag/AgCl). The polarization tests were repeated at least three times for each specimen. The corrosion potential (E_{corr}) and corrosion current density (I_{corr}) were determined from the registered curves by the extrapolation method.

3. Results and discussion

3.1 *Microstructure and X-ray diffraction (XRD) analysis*

The present alloy which is called as 'metastable-β-alloy' subjected to thermo-mechanical processing exhibited various microstructure on heat treatment. Microstructure observations of the as-cast sample performed using optical microscopy (OM) and SEM showed the presence of fine needle-like α-phase (acicular α) in former β-phase matrix with segregation of α phase on grain boundaries (figure 3a and b). For each former β-grain, 12 different crystal orientations of the α-precipitates (variants) are available according to the Burgers relationship,[47] which links particular crystal directions and planes of both phases:

$$\langle 111\rangle_{\beta} // \langle 1120\rangle_{\alpha}, (110)_{\beta} // (0001)_{\alpha}.$$

These phase constitutions were identified from XRD spectra as shown in figure 4. XRD profiles revealed peaks corresponding to only α and β phases in as-cast TNZV alloy.

The microstructure of an investigated TNZV alloy depends essentially upon both the plastic deformation process and heat treatment sequences imposed on it. In the present study, thermo-mechanical processing was carried out by performing 10% forging plus 25% rolling at 650°C (below β-transus) is a heavy deformation (>30%) which is an effective process to create worked structure in the alloy and nucleate α-phase during the plastic deformation.[41,42] It is well known that the primary α (hcp) is one of the microstructural features in Ti alloys that remains untransformed during solution treatment in the α + β phase field (650°C). The thermo-mechanical processing plays an effective role to alter the morphology of primary α which can be lamellar,equiaxed or mixed.[48,49] It is expected that plastic deformation in the α + β phase

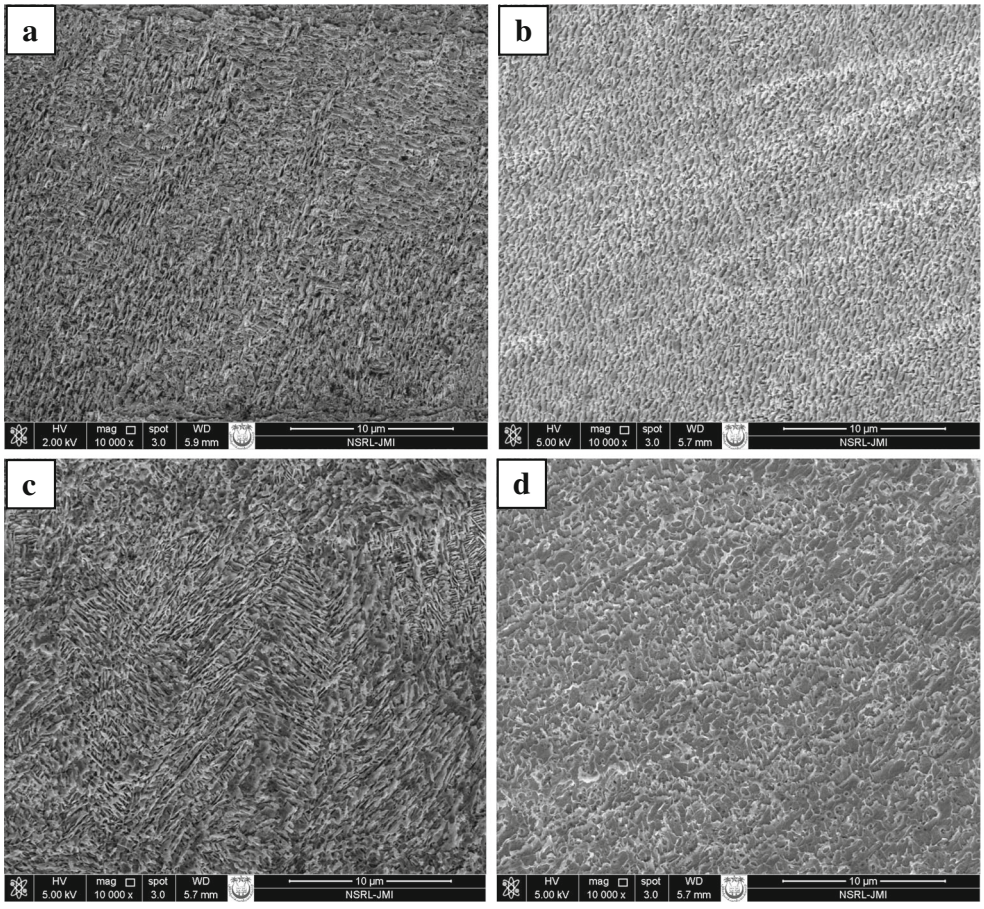

Figure 5. Scanning electron microstructures (10,000×) of the TNZV alloy deformed at 650°C and solution treated at same temperature for 1 h followed by (**a**) furnace cooling (FC), (**b**) air cooling (AC), (**c**) water quenching (WQ) and (**d**) aging of WQ samples at 500°C for 5 h.

field produces dislocation density which serves as nucleation sites of α phase during subsequent cooling to room temperature. At the same time, furnace cooling after solution treatment at 650°C encourages the phase transformation of the β-phase into α-phase and forms a large number of α phase nucleation sites. Hence, subsequent solution treatment at 650°C with a long holding time of 1 h followed by furnace cooling increased significantly the volume fraction of α phase and resulted in the recrystallization of any elongated α that may have formed during hot working at 650°C. Consequently, the presence of primary equiaxed α and transformed β within pre-existing β phase was seen in the furnace cooled (FC) samples solution treated at 650°C (figures 5a and 6a). In case of the air cooling (AC) after solution treatment at 650°C, the microstructure consists of primary α and transformed β on a very fine scale. During this treatment, a part of the β-transformed into α and formed large number of nucleation sites as shown in figures 5b and 6b. It can be seen that all the furnace cooled and air cooled TNZV samples consisted of α- and β-phases. The samples subjected to deformation and solution treatment at 650°C followed by water quenching (WQ) consists of fine scale elongated/globular α and retained β-phase as matrix. Partial recrystallization of deformed α may happen owing to faster cooling (figures 5c and 6c). Considerable literature is reported[27,41,42,49–54] which confirms the presence of martensite structure in Ti materials if the solution treatment has been done at high temperature (above β-phase field) with sufficiently high cooling rate. Hence, it is impossible here to produce martensite phase in the microstructure after fast cooling (WQ) from the below temperature (650°C in this case). It is reported that partitioning of alloying elements occurs during solution treatment at below transus temperature along with β- to α-transformation.[30,41,42,49] The distribution of the alloying elements depends upon their solubility, diffusion rate, as well as the time allowed for diffusion to take place.[56] Therefore, β-phase becomes enriched with Nb and Zr elements during this treatment which lead to reduces the martensite start temperature (M_s) of the untransformed β to below room temperature[30] and thus no martensite was created on water quenching from 650°C.

The aging process of the WQ samples subjected to deformation and solution treatment at 650°C established considerable growth of α from β phases (figures 5d and 6d). Moreover, aging modified the morphology of the elongated α into equiaxed α.

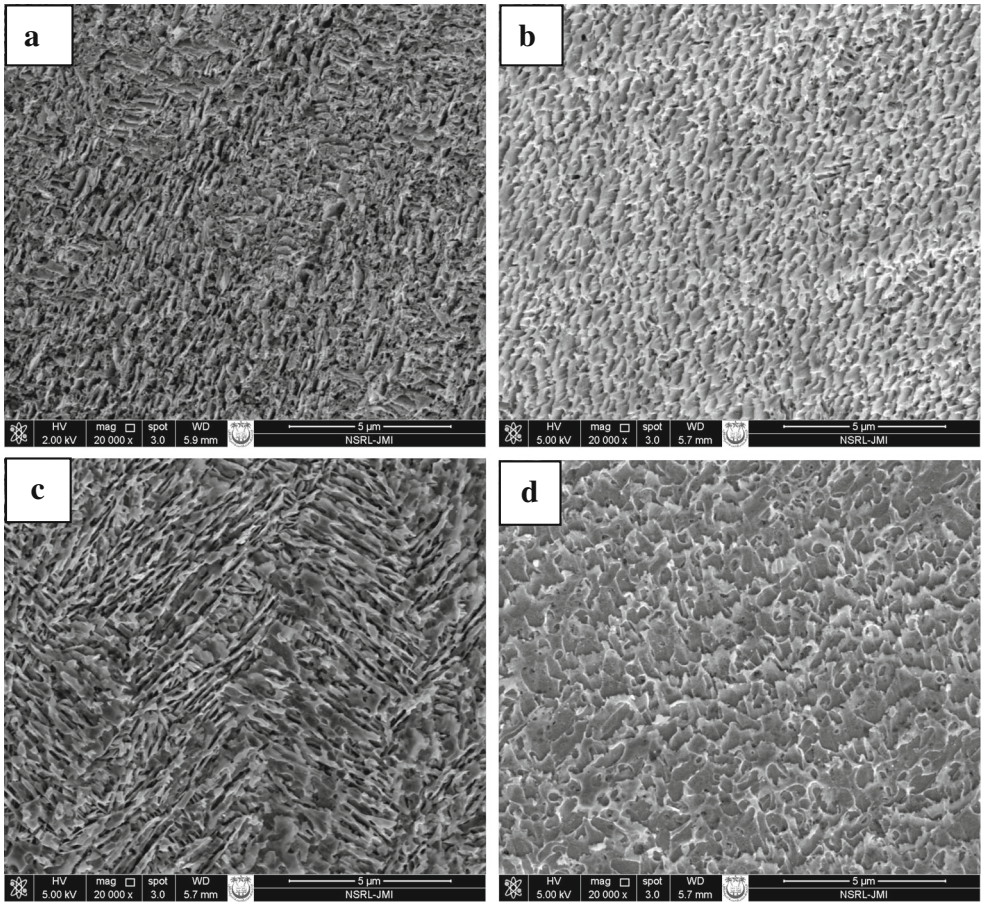

Figure 6. Scanning electron microstructures (20,000×) of the TNZV alloy deformed at 650°C and solution treated at same temperature for 1 h followed by (**a**) furnace cooling, (**b**) air cooling, (**c**) water quenching and (**d**) aging of WQ samples at 500°C for 5 h.

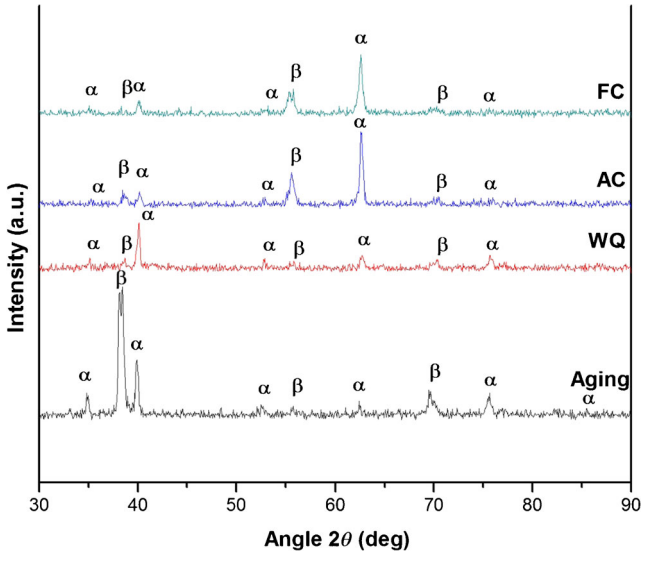

Figure 7. X-ray diffraction profiles of TNZV alloy deformed at 650°C and solution treated at same temperature for 1 h followed by furnace cooling (FC), air cooling (AC), water quenching (WQ) and aging of WQ samples at 500°C for 5 h.

The presence of different phases was further confirmed using the XRD spectra as shown in figure 7. The presence of peaks of α and β phases in all the heat treated conditions were observed.

3.2 *Mechanical properties*

3.2a *Hardness*: The effect of heat treatment on microhardness of the TNZV samples is presented in figure 8. Solution treatment in the $\alpha + \beta$ field (at 650°C) followed by furnace cooling showed higher hardness compared with water cooled samples due to higher amount of α-phase. Amongst all solution treatment conditions, air cooled samples established higher hardness than the furnace cooled and water quenched samples owing to relatively fast cooling which formed finer phases. On other hand, the water quenched samples presented a substantial decrease in hardness (HV= 230 ± 2). However, in the case of the aged samples, aging treatment had a valuable effect on hardness by increasing its value to (HV = 269 ± 4). Many authors[13,41,42,55,58] mentioned that substantial enhancement in hardness can be achieved after aging treatment. This heat treatment process

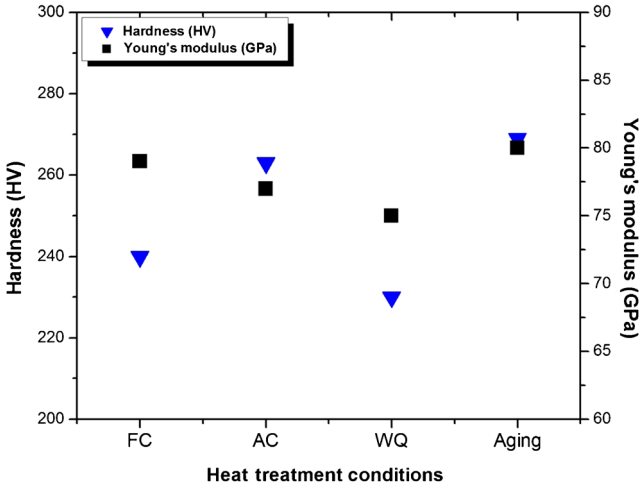

Figure 8. Vickers hardness and Young's modulus of TNZV alloy deformed and solution treated at same temperature for 1 h followed by furnace cooling (FC), air cooling (AC), water quenching (WQ) and aging of WQ samples at 500°C for 5 h.

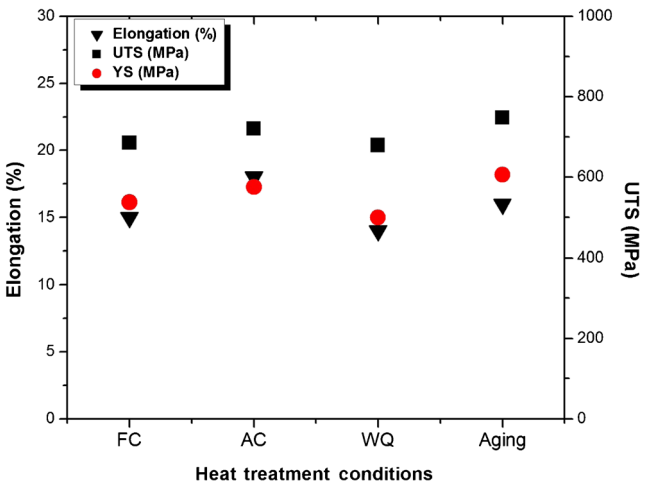

Figure 9. Tensile properties of TNZV alloy deformed at 650°C and solution treated at same temperature for 1 h followed by furnace cooling (FC), air cooling (AC), water quenching (WQ) and aging of WQ samples at 500°C for 5 h.

has ability to precipitate α-phase in the matrix by decomposition of retained β-phase and/or martensite, this precipitates of the α-phase in the matrix increases the hardness of the TNZV alloy. Therefore, this increase in hardness of aged samples is associated with the increase in volume fraction of α-phase as a result of more decomposition of some amount of retained β into α.

3.2b *Elastic modulus*: Young's modulus is determined by the bonding force among atoms and greatly affected by the phase/crystal structure[16] and chemical composition of Ti material.[27,57] Therefore, the specific modulus of the phases and by their volume fractions in any multiphase Ti alloy is a key parameter to develop the modulus. It is well known that the composition of the constituent phases and their volume fractions depend mainly upon the history of thermal and thermo-mechanical processing.[59] It has been reported that the elastic modulus of the phases of Ti alloys increases in the sequence $E_\beta < E_{\alpha''} < E_\alpha < E_\omega$.[16,27,50,60] It is inferred that the microstructure of Ti alloys plays a significant role in reducing the modulus as the β and α'' phase mixture lower the elastic modulus whereas the α phase increases it.[27,61] In general, low elastic modulus are supposed to be contradictory aspects for specific solid materials, particularly for metals and alloys in biomedical applications. Young's modulus must be close to that of the bone (around 30 GPa for the cortical bone), which minimizes the bone atrophy because of the stress shielding effect and accordingly an increase in the durability of the implant in service is expected. The modulus of elasticity of TNZV alloy samples subjected to different heat treatment conditions is presented in figure 8. The elastic modulus of the heat treated TNZV samples varied from 75 ± 2.2 to 79 ± 1.7 GPa. The microstructure of the furnace cooled, air cooled and water quenched samples consisted of α and β phases. However, furnace cooled samples have higher elastic modulus than air cooled samples. This is due to the higher volume fraction of α phase in the furnace cooled samples (figures 5a and 6a) as a result of slower cooling during which α-phase has adequate time to grow. In case of water quenched samples, a noticeable reduce in Young's modulus was seen compared with furnace cooled and air cooled samples. This can be attributed to the fastest cooling rate which can suppress more transformations of β-phase to α-phase and also this type of cooling prevents the growing of α-phase as a result of insufficient time. Therefore, the presence of higher amount of retained β-phase provided the lowest value of elastic modulus (75 ± 2.2 GPa) regardless of the absence of any low modulus α'' martensite in the microstructure. Aging at 500°C for 5 h after water quenching from 650°C resulted in the more decomposition of retained β-phase to α-phase in the microstructure. This decomposition led to increase Young's modulus substantially (80 ± 2.7 GPa). This value of Young's modulus is comparable to the modulus of furnace cooled samples owing to high amount of α-phase.

3.2c *Tensile properties*: In general, high mechanical properties are supposed to be contradictory aspects for specific solid materials, particularly for metals and alloys in biomedical applications. The high yield strength is necessary for the implants to meet the complex stresses including tension, compression, bending and torsion which are applied to the implants during the routine activities. Moreover, the elongation of metallic materials for biomedical applications is required to be more than 10 pct.[26] The tensile test data was obtained for the TNZV samples deformed at 650°C and solution treated at the same temperature followed by water quenching, air cooling or furnace cooling. Accordingly, the yield strength (YS) represented by 0.2% proof stress, ultimate tensile strength (UTS) and fracture plasticity (total elongation to failure) are presented in figure 9. The figure

shows that the UTS, YS and elongation of these samples varied from 679 to 720 MPa, 500 to 575 MPa and 14–18%, respectively. On other hand, the UTS, YS and elongation of the aged samples were 748, 606 MPa and 16%, respectively. In the current study, it can be observed that the trend of the variation of UTS with heat treatment conditions was analogous to that of hardness (figures 8 and 9).

Solution treatment at 650°C ($\alpha + \beta$ field) followed by furnace cooling showed low tensile strength compared with air cooled samples in spite of higher amount of α-phase. The air cooled samples established higher strength (YS and UTS) and ductility than the furnace cooled and water quenched samples owing to relatively fast cooling which formed finer microstructure consists from equiaxed primary α and transformed β (figures 5b and 6b). On other hand, the water quenched samples presented a reasonable value of tensile strength (UTS = 679 MPa) as a result of presence α phase in the microstructure (figures 5c and 6c). However, in the case of the aged samples, aging treatment had a valuable effect on strength by increasing UTS and YS to 748 and 606 MPa, respectively. This increasing of strength properties in aged samples is associated with the increase in volume fraction of α-phase as a result of more decomposition of some amount of retained β-phase into α-phase. It can be seen that aging treatment of water quenched samples presented an increase in ductility of water quenched samples owing to the change of morphology of α-phase from elongated to equiaxed structure as shown in figures 5d and 6d.

3.3 *Electrochemical properties*

3.3a *Open-circuit potential*: Figure 10 represents the variation of OCP of TNZV alloy in different heat treatment conditions as a function of immersion time in naturally aerated Ringer's solution at 37°C, until its variation with time became negligible. The steady-state OCP of TNZV alloy varies with heat treatment conditions.

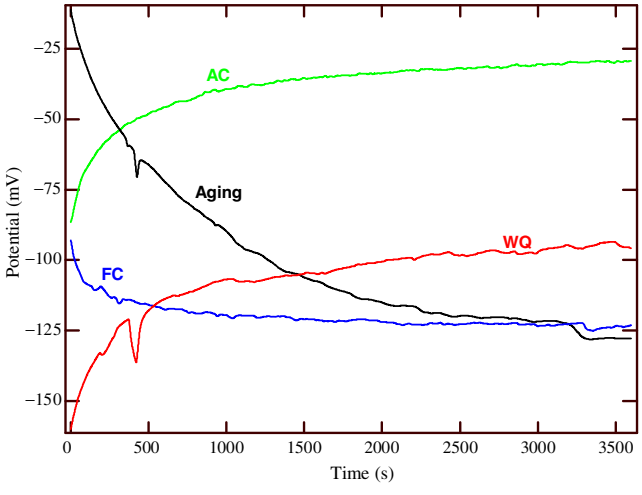

Figure 10. Open-circuit potential *vs.* time curves of the TNZV alloy in Ringer's solution at 37°C deformed at 650°C and solution treated at same temperature for 1 h followed by furnace cooling (FC), air cooling (AC), water quenching (WQ) and aging of WQ samples at 500°C for 5 h.

By comparing the results depicted in figure 10, it can be observed that the air cooled samples present the most positive corrosion potential values (nobler behavior) than that of furnace cooled samples, water quenched samples and also after aging of WQ samples. In the present study, among all the heat treated samples, the furnace cooled and aged samples showed a substantial decrease in OCP. In addition, the OCP curve of WQ samples and aging of WQ samples exhibited the fluctuations in the initial stage and then became stable. On other hand, the AC and WQ samples showed tendency of spontaneous formation of surface oxides and a continuous shifting towards noble (positive) direction when they were in contact with Ringer's solution. It can be observed that the time profiles of the OCP are characteristic of passive film formation, especially in the stabilized region, on the alloy surfaces immersed in aerated solutions in different heat treatment conditions.[62] AC samples, however, displayed the greatest tendency to spontaneous oxide film formation in Ringer's solution. The OCP values for all heat treatment conditions show an overall increase for the time duration of 1 h, indicating that their corrosion resistance increases with time and reaches a relatively stable value. In other words, the OCP shifts in the positive direction which indicates the formation of protective passive oxide film on the surface of the TNZV alloy.

The protective passive film forms rapidly and acts as a barrier for metal dissolution, reducing the corrosion rate. The thickness of the spontaneously formed protective oxide film on surfaces of Ti and its alloys has been reported as 1–4 nm at open-circuit conditions.[63] It is well known that the superior corrosion behavior of Ti and its alloys is caused by the spontaneous creation of a tightly adherent protective oxide film on their surface even in solutions with low oxygen contents.[64] Oliveira *et al*[65] reported an instance of an oxide film creation on Ti–13Zr–13Nb and Ti–50Zr alloys in aerated solution. It is reported in the literature that X-ray photo-electron spectroscopy (XPS) reveals that the formed amorphous oxide film mainly consists of TiO_2[68] in addition to two types of oxides: TiO and Ti_2O_3.[25,66,67] It has also been found that the oxides of titanium, TiO or Ti_2O_3, transform to more stable TiO_2 and come out on the electrode/electrolyte interface after a direct contact between Ti material and the electrolyte.[33] TiO_2 is an *n*-type semiconductor[69] and the corrosion of Ti is controlled kinetically by migration of oxygen vacancies through this film.[72] Hence, the corrosion behavior reached to a relatively stable state as the corrosion resistance of the electrode enhanced ultimately. The decrease of the anodic dissolution current of Ti alloy and shifting the OCP gradually in the positive direction are the normal results of corrosion resistance increase.

It is important to mention here that many researhers[63,70,71,73] found that the film formed on the surface of Ti and its alloys in various physiological solutions showed a two-layered structure comprising of a dense inner layer and a porous

outer layer. The excellent corrosion behavior of the materials is essentially because of the barrier of inner layer which presents high resistance.[62,70]

Many authors[66,74–77] ensured that the passive film in Ti–Nb–Zr alloy system consists principally of TiO_2 with a trace quantity of Nb_2O_5 and ZrO_2. The presence of Nb_2O_5 or ZrO_2 with the main passive TiO_2 layer develops the structural integrity of the oxide film and enhances its resistance to dissolution.[66,78] For example, the presence of Nb cations enhances the passivation properties of the surface film by decreasing the concentration of anion vacancies present on Ti oxide film. These anion vacancies are generated by the presence of lower Ti oxidation states.[46,66,79] Robin *et al*[62] proved through an electrochemical study that the high corrosion resistance of Ti–*x*Nb–13Zr alloy depends mainly on the resistance of the homogeneous barrier inner layer formed on the alloy in Ringer's solution at 37°C. Moreover, it has also been pointed out that the inner layer formed on the surface of Ti–Nb–Zr alloy system is apparently more protective in comparison to other alloy systems as a result of the less porous passive film formed.[70]

3.3b *Potentiodynamic polarization*: Figure 11 shows the potentiodynamic anodic polarization curves of different heat-treated TNZV samples as measured with respect to saturated calomel electrode (SCE) in naturally aerated Ringer's solution at 37°C. The continuity, stability and intensity of the passive Ti oxide film are analyzed by this technique. As can be seen, the polarization curves obtained for the investigated TNZV alloy samples in all heat treatment conditions show a typical active–passive characterization, a rising anodic current with increasing potential and then transforming directly into the passive area from the Tafel curves. The passive current densities for the investigated TNZV alloy samples in all heat treatment conditions remained constantly with increasing potential that reveal the thickening of its passive layer.[20]

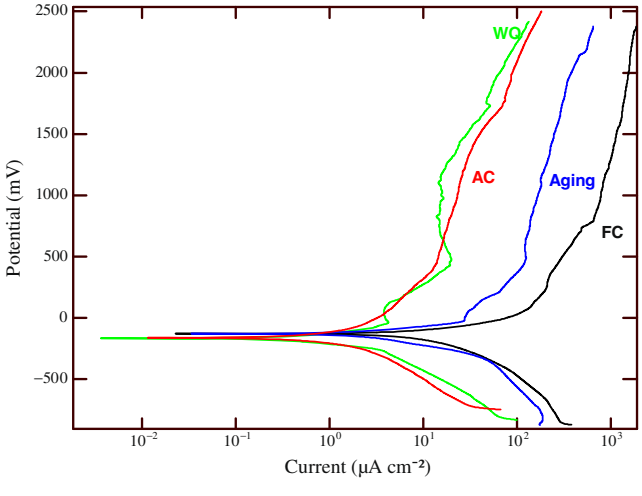

Figure 11. Cyclic polarization behavior of the TNZV alloy in Ringer's solution at 37°C deformed at 650°C and solution treated at same temperature for 1 h followed by furnace cooling (FC), air cooling (AC), water quenching (WQ) and aging of WQ samples at 500°C for 5 h.

The average corrosion potentials (E_{corr}) can be estimated from these curves as −133.97, −171.51, −171.64, −137.74 mV (*vs.* SCE) for the furnace cooled samples, air cooled samples; water quenched samples and aged samples, respectively. The corrosion potentials determined from the polarization curves are significantly lower than those obtained from the open circuit potentials measurements. This is expected, as the polarization tests were started at a cathodic potential relatively to the corrosion potential, so that the surface passive oxide film was at least partially removed due to the highly reducing initial potentials.

The mean corrosion current densities (I_{corr}) and corrosion rates were obtained for investigated TNZV alloy by Tafel extrapolation analysis method using both anodic and cathodic branches of the polarization curves as shown in figure 12. The corresponding corrosion data which include the mean corrosion current densities (I_{corr}), corrosion potentials (E_{corr}), and corrosion rates of TNZV alloy in different heat treatment conditions are given in table 2.

From the above corrosion test results, it can be observed that in most of the heat treatment conditions, the corrosion potential (E_{corr}) varied roughly within a narrow range. In

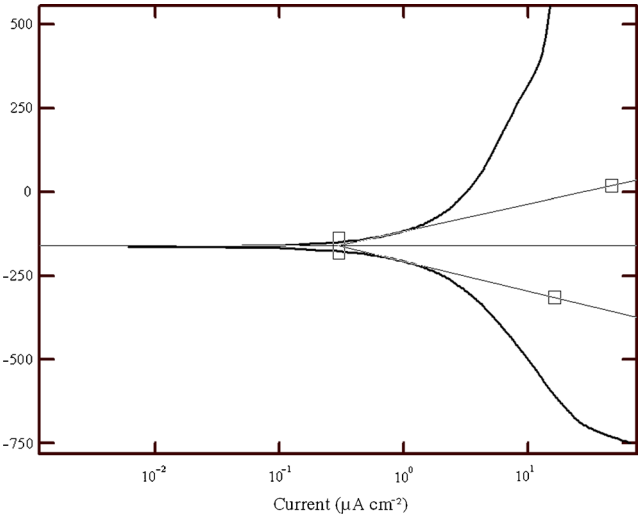

Figure 12. Tafel plots obtained on furnace cooled sample in Ringer's solution at 37°C.

Table 2. Results of electrochemical tests *via* the anodic polarization curves of the heat-treated TNZV alloy in Ringer's solution at 37°C.

Cooling conditions	E_{corr} (mV)	I_{corr} (μA cm^{-2})	Corrosion rate (mils per yr)
FC	−133.97	12.8104	10.4
AC	−171.51	0.7983	0.65
WQ	−171.64	0.7776	0.63
Aging	−137.74	2.3685	1.9

general, air cooled samples and water quenched samples resulted further decrease in the E_{corr} value and it was lower than that of the furnace cooled samples and aged samples. The air cooled samples and water cooled samples showed comparable E_{corr} values whilst furnace cooled and aged samples were also in almost analogous E_{corr} values.

Comparing the four anodic curves, however, it can be noticed that the furnace cooled samples and aged samples exhibited similar anodic polarization behaviors, including high current densities of 12.8104 and 2.3685 μA cm^{-2}, respectively, at approximately 2500 mV (Ag/AgCl). On other hand, the air cooled samples and water quenched samples showed comparable current densities of 0.7983 and 0.7776 μA cm^{-2}, respectively, at approximately 2500 mV (Ag/AgCl).

As mentioned in OCP analysis, as soon as the TNZV samples are rinsed in Ringer's solution a protective surface oxide film is formed on the surface of samples and they get passivated which is also reproduced in the anodic polarization curves (figure 11).

The corrosion current density of the furnace cooled samples presented the highest comparing with of air cooled and water quenched samples. Moreover, the anodic current densities of air cooled samples and water quenched samples are lower than of the furnace cooled samples and aged samples. This indicates that among all the samples which were subjected to deformation and solution treatment at 650°C, the minimum corrosion current density was observed in case of air cooled samples and water cooled samples (figure 11) as the surface film formed on the air cooled and water quenched samples is more compact and protective. Consequently, this implies that the anodic current density of TNZV alloy in all heat treatment conditions increases with increase in the potential, but this increase is always larger for the furnace cooled samples and aged samples. The rise in current density with the potential is likely because of the insufficient increase in oxide film thickness with potential to re-compensate the increase in potential. It is reported that this current increase could be associated with the oxidation of TiO and Ti_2O_3 to TiO_2.[66] Thus, it appears that the surface oxide films thicken to compensate the increase in potential where the current does not change with potential.

In the current research, it is expected that the fine ($\alpha + \beta$) structure in the matrix of air cooled samples increases the α/β interface area and then accelerates the galvanic corrosion of the alloy. Regardless of this, air cooled samples showed lower corrosion current density and corrosion rate compared to the furnace cooled or aged samples. It has been revealed that the corrosion behavior of CP-Ti (single α-phase) was lower than that of Ti–6Al–7Nb alloy ($\alpha+\beta$).[80] Therefore, the foremost reason of this better corrosion behavior of air cooled samples is due to the small amount of less noble α-phase in their microstructures. Further, the microstructure analysis of SEM and XRD tests did not revealed any martensite formed in the water quenched samples after solution treatment at 650°C (figures 5c, 6c and 7). The harmful corrosion behavior of the high amount of strain energy which is coupled with the martensite formation[81] will not be happened as the microstructure consists of α- and β-phases only. Thus, no significant change in corrosion current density is found between air cooled and water quenched samples. The water quenched samples have improved corrosion stability (lower I_{corr}) as a result of the formation of a more stable passive film than furnace cooled or aged samples owing to the less amount of less noble phase (α) in the microstructure.

The researches related the higher corrosion behavior of the Ti–Nb–Zr alloy system when Nb_2O_3 and ZrO_2 are represented in passive inner TiO_2 layer which work as inhibitor to adsorption of Cl^- ions into the oxide film and in turn increase the structural integrity of the oxide film.[65,71] Also, it is proved[62] that the resistance of a compact oxide film formed on the Ti–13Nb–13Zr alloy is higher than that measured for Ti–6Al–4V alloy. This inference is derived from the fact that the presence of alloying elements in the Ti materials encourages the creation of ions like Nb^{5+} that increase the number of oxygen ions and cancel out the anion vacancies which make the film more stable and protective.[79]

Aging treatment of water quenched samples created higher amounts of precipitates of less noble α-phase in the microstructure as some part of the retained β-transforms into α (figures 5d and 6d). Thus, in the same way, the α/β interface increased with the increase of α-phase volume friction which in turn led to an increase in corrosion current density (I_{corr}) from 0.7776 to 2.3685 μA cm^{-2}.

4. Conclusion

The effect of thermo-mechanical processing on microstructure, mechanical properties and electrochemical behavior of metastable-β Ti–20.6Zr–13.6Nb–0.5V alloy for biomedical applications has been investigated. After the analysis of the results, following conclusions are drawn:

1. The microstructure of the thermo-mechanical treated TNZV alloy consists mainly of equiaxed/elongated α, β-phases with different morphologies depending upon the heat treatment conditions.
2. Air cooled samples show higher hardness, strength (UTS, YS), and elongation than furnace cooled or water quenched samples.
3. Water quenched samples introduce lower Young's modulus (75 ± 2.2 GPa) compared to other heat treated samples due to less amount of α-phase in the microstructure.
4. Aging treatment of WQ samples led to increase in the hardness, strength, elastic modulus and elongation.
5. Corrosion tests indicated that TNZV alloy undergoes spontaneous passivation owing to spontaneously formed oxide film in the human body environment.
6. The air cooled and water quenched samples showed lower corrosion rate owing to the less amount of less noble phase-α in the microstructure.

7. According to the presented results it could be considered that the mechanical properties and corrosion behavior of investigated TNZV alloy suggest that the alloy is appropriate for biomedical applications.

Acknowledgements

MTB would like to sincerely acknowledge the financial assistance provided by the Government of Iraq, Ministry of High Education and Scientific Research. He would also like to thank the Iraqi Cultural Office, New Delhi, India and Indian Council of Cultural Relations (ICCR), New Delhi, India, for supporting him during the period of his Ph.D. program. Many thanks to Defense Metallurgical and Research Laboratories-Hyderabad, India for helping us with manufacturing cast Ti alloy.

References

1. Cremasco A, Osorio W R, Freire C M A, Garcia A and Caram R 2008 *Electrochim. Acta* **53** 4867
2. Long M and Rack H J 1998 *Biomaterials* **19** 1621
3. Wang K 1996 *Mater. Sci. Eng. A* **213** 134
4. Boehlert C J 1999 *Mater. Sci. Eng. A* **267** 82
5. Niinomi M 2003a *Sci. Technol. Adv. Mater.* **4** 445
6. Niinomi M 2003b *Biomaterials* **24** 2673
7. Mythili R, Thomas Paul V, Saroja S, Vijayalakshmi M and Raghunathan V S 2005 *Mater. Sci. Eng. A* **390** 299
8. Hanawa T 2006 *Mater. Sci. Forum* **512** 243
9. Brojan D, Fajfar P, Kosel F and Turk R 2007 *RMZ Mater. Geoenviron.* **54** 471
10. Yu J, Zhao Z J and Li L X 1993 *Corros. Sci.* **35** 587
11. Okazaki Y, Ito Y, Kyo K and Tateishi T 1996 *Mater. Sci. Eng. A* **213** 138
12. Rao S, Okazaki Y, Tateishi T, Ushida T and Ito Y 1997 *Mater. Sci. Eng. C* **4** 311
13. Ikeda M, Komatsu S-Y, Sowa I and Niinomi M 2002 *Metall. Mater. Trans.* **A33** 487
14. Sumner D and Galante J 1992 *Clin. Orthop. Relat. Res.* **274** 202
15. Gasser B 2001 *Design and engineering criteria for titanium devices, titanium in medicine* (German: Springer)
16. Ho W, Ju C and Chern Lin J 1999 *Biomaterials* **20** 2115
17. Park C-H, Park J W, Yeom J T, Chun Y S and Lee C S 2010 *Mater. Sci. Eng. A* **527** 4914
18. Zysett P K, Guo X E, Hoffler C E, Moore K E and Goldstein S A 1998 *Tech. Health Care* **6** 429
19. Nang S, Banerjee R, Stechschulte J and Fraser H L 2005 *J. Mater. Sci. Mater. Med.* **16** 679
20. Karthega M, Raman V and Rajendran N 2007 *Acta Biomater.* **3** 1019
21. Raabe D, Sander B, Friak M, Ma D and Neugebauer J 2007 *Acta Mater.* **55** 4475
22. Niinomi M 2002 *Met. Mater. Trans.* **33A** 477
23. Ikehata H, Nagasako N, Furuta T, Fukumoto A, Miwa K and Saito T 2004 *Phys. Rev. Condens. Matter* **B70** 174113:1
24. Abdel-Hady M, Hinoshitaa K and Morinagaa M 2006 *Scr. Mater.* **55** 477
25. Been J and Grauman J S 2000 *Titanium and titanium alloys* (ed) R W Revie (New York: NY: John & Wiley Inc.)
26. Niinomi M 1998 *Mater. Sci. Eng. A* **243** 231
27. Collings E W 1984 *Physical metallurgy of titanium alloys* (OH: ASM, Metals Park)
28. Niinomi M, Akahori T, Takeuchi T, Katsura S, Fukui H and Toda H 2005 *Mater. Sci. Eng. C* **25** 417
29. Zhang R G and Acoff V L 2007 *Mater. Sci. Eng. A* **463** 67
30. Tang X, Ahmed T and Rack H J 2000 *J. Mater. Sci.* **35** 1805
31. Ribeiro A L R, Junior R C, Cardoso F F, Filho R B F and Vaz L G 2009 *J. Mater. Sci.: Mater. Med.* **20** 1629
32. Kim J I, Kim H Y, Inamura T, Hosoda H and Miyazaki S 2005 *Mater. Sci. Eng. A* **403** 334
33. Sun F, Hao Y L, Nowak S, Gloriant T, Laheurte P and Prima F 2011 *J. Mech. Behav. Biomed. Mater.* **4** 1864
34. Yang G and Zhang T 2005 *J. Alloys Compd.* **392** 291
35. Degarmo Paul E, Black J T and Kohser Ronald A 2003 *Materials and processes in manufacturing* (German: Wiley)
36. Weaver M L and Garmestani H 1998 *Mater. Sci. Eng. A* **247** 229
37. Bache M R and Evans W J 2001 *Mater. Sci. Eng. A* **319–321** 409
38. Lonardelli I, Gey N, Wenk H R, Humbert M, Vogel S C and Lutterotti L 2007 *Acta Mater.* **55** 5718
39. Ding R, Guo Z X and Wilson A 2002 *Mater. Sci. Eng. A* **327** 233
40. Geetha M, Mudali U K, Gogia A K, Asokamani R and Baldev R 2004 *Corros. Sci.* **46** 877
41. Majumdar P, Singh S B and Chakraborty M 2011a *J. Mech. Behav. Biomed. Mater.* **4** 1132
42. Majumdar P, Singh S B, Chatterjee U K and Chakraborty M 2011b *J. Mater. Sci.: Mater. Med.* **22** 797
43. Kuhn H and Medlin D 1972 *Mechanical testing and evaluation* (OH: ASM International)
44. Gonzalez J E G and Mirza-Rosca J C 1999 *J. Electroanal. Chem.* **471** 109
45. Oliveira N T C, Biaggio S R, Rocha-Filho R C and Bocchi N 2005 *J. Biomed. Mater. Res.* **74** 397
46. Rosalbino F, Macciò D, Scavino G and Saccone A 2012 *J. Mater. Sci.: Mater. Med.* **23** 865
47. Burgers W 1934 *Physica* **1** 561
48. Banergee D and Krishnan R V 1981 (eds) S Ranganathan, V S Arunachalam and R W Cahn (Bangalore: Indian Academy of Sciences)
49. Boyer R, Welsch G and Collings E W 1994 *Materials properties handbook: titanium alloys* (Ohio: ASM International)
50. Hao Y L, Niinomi M, Kuroda D, Fukunaga K, Zhou Y L, Yang R and Suzuki A 2002 *Metall. Mater. Trans.* **A33** 3137
51. Mantani Y and Tajima M 2006 *Mater. Sci. Eng. A* **438–440** 315
52. Banumathy S, Prasad K S, Mandal R K and Singh A K 2011 *Bull. Mater. Sci.* **34** 1421
53. Ahmed T and Rack H J 1996 *J. Mater. Sci.* **31** 4267
54. Taekyung Lee, Yoon-Uk Heo and Chong Soo Lee 2013 *Scr. Mater.* **69** 785

55. Kuroda D, Kawasaki H, Yamamoto A, Hiromoto S and Hanawa T 2005 *Mater. Sci. Eng. C* **25** 312
56. Mansur Ahmed, Azdiar A, Dmytro G, Orest M and Elena V 2012 *J. Mater. Sci.* **47** 7013
57. Song Y, Xu D S, Yang R, Li D, Wu W T and Guo Z X 1999 *Mater. Sci. Eng. A* **260** 269
58. Slokar L, Matković T and Matković P 2012 *Mater. Des.* **33** 26
59. Lee Y T and Welsch G 1990 *Mater. Sci. Eng. A* **128** 77
60. Majumdar P, Singh S B and Chakraborty M 2008 *Mater. Sci. Eng. A* **489** 419
61. Cui W F and Guo A H 2009 *Mater. Sci. Eng. A* **527** 258
62. Robin A, Carvalho O A S, Schneider S G and Schneider S 2008 *Mater. Corros.* **59** 929
63. Marino C E B, Oliveira E M, Rocha-Filho R C and Biaggio S R 2001 *Corros. Sci.* **43** 1465
64. Okazaki Y, Tateishi T and Ito Y 1997 *Mater. Trans. JIM* **38** 78
65. Oliveira N T C, Ferreira E A, Duarte L T, Biaggio S R, Rocha-Filho R C and Bocchi N 2006 *Electrochim. Acta* **51** 2068
66. Yu S Y and Scully J R 1997 *Corrosion* **53** 965
67. Pouilleau J, Devilliers D, Garrido F, Durand-Vidal S and Mahé E 1997 *Mater. Sci. Eng. B* **47** 235
68. Narayanan R and Seshadri S K 2008 *Corros. Sci.* **50** 1521
69. Pan J, Leygraf C, Thierry D and Ektessabi A M 1997 *J. Biomed. Mater. Res.* **35** 309
70. Assis S L and Costa I 2007 *Mater. Corros.* **58** 329
71. Assis S L, Wolynec S and Costa I 2008 *Mater. Corros.* **59** 739
72. Hong S B, Eliaz N, Sachs E M, Allen S M and Latanision R M 2001 *Corros. Sci.* **43** 1781
73. Alves V A, Reis R Q, Santos I C B, Souza D G, Goncalves T de F, Pereira-da-Silva M A, Rossi A and da Silva L A 2009 *Corros. Sci.* **51** 2473
74. Manivasagam G, Mudali U K, Asokamani R and Raj B 2003 *Corros. Rev.* **21** 125
75. Choubey A, Basu B and Balasubramaniam R 2005 *Trends Biomater. Artif. Organs* **18** 64
76. Jun L I, Lian Zhou and Zuoochen L I 2010 *Rare Met.* **29** 37
77. Bai Y, Li S J, Prima F, Hao Y L and Yang R 2012 *Appl. Surf. Sci.* **258** 4035
78. Geetha M, Singh A K, Asokamani R and Gogia A K 2009 *Prog. Mater. Sci.* **54** 397
79. Metikoš-Huković M, Kwokal A and Piljac J 2003 *Biomaterials* **24** 3765
80. Raman V, Tamilselvi S, Nanjundan S and Rajendran N 2005 *Trends Biomater. Artif. Organs* **18** 137
81. Wayman C M and Bhadeshia H K D H 1996 *Physical metallurgy* (eds) R W Cahn and P Haasen (Amsterdam: Elsevier Science Publishers)